

## Apparent beam size definition of focused ion beams based on scanning electron microscopy images of nanodots

Nikola Vladov, Joel Segal, and Svetan Ratchev

Citation: [Journal of Vacuum Science & Technology B](#) **33**, 041803 (2015); doi: 10.1116/1.4926388

View online: <http://dx.doi.org/10.1116/1.4926388>

View Table of Contents: <http://scitation.aip.org/content/avs/journal/jvstb/33/4?ver=pdfcov>

Published by the AVS: Science & Technology of Materials, Interfaces, and Processing

---

### Articles you may be interested in

[Self-assembly of well-aligned 3 C - Si C ripples by focused ion beam](#)

*Appl. Phys. Lett.* **92**, 193107 (2008); 10.1063/1.2927473

[Morphological instability of Cu nanolines induced by Ga + -ion bombardment: In situ scanning electron microscopy and theoretical model](#)

*J. Appl. Phys.* **103**, 074306 (2008); 10.1063/1.2903881

[Advanced nanoscale material processing with focused ion beams](#)

*J. Vac. Sci. Technol. B* **22**, 2995 (2004); 10.1116/1.1813467

[Focused ion beam induced surface amorphization and sputter processes](#)

*J. Vac. Sci. Technol. B* **21**, 927 (2003); 10.1116/1.1565345

[Focused ion beam sputter yield change as a function of scan speed](#)

*J. Vac. Sci. Technol. B* **15**, 2346 (1997); 10.1116/1.589643

---



**WE'RE SEARCHING FOR**  
**SKILLED ANTENNA, RF SYSTEMS AND MICROWAVE DESIGN ENGINEERS.**  
HELP US ENGINEER A BETTER TOMORROW. [LEARN MORE](#)

**LOCKHEED MARTIN**

# Apparent beam size definition of focused ion beams based on scanning electron microscopy images of nanodots

Nikola Vladov,<sup>a)</sup> Joel Segal, and Svetan Ratchev

*Institute of Advanced Manufacturing, Faculty of Engineering, University of Nottingham, University Park, Nottingham NG7 2RD, United Kingdom*

(Received 6 May 2015; accepted 24 June 2015; published 6 July 2015)

In this paper, the new term *apparent beam size* of focused ion beam (FIB) is introduced and an original method of its evaluation is demonstrated. Traditional methods of measuring the beam size, like the knife edge method, provide information about the quality of the beam itself, but practically, they do not give information on the FIB sputtering resolution. To do this, it is necessary to take into account the material dependent interaction of the beam with the specimen and the gas precursor in the vacuum chamber. The apparent beam size can be regarded as the smallest possible dot that FIB can sputter in a given specimen. The method of evaluating it, developed in this paper, is based on the analysis of a series of scanning electron images of FIB produced nanodots. Results show that the apparent beam size can be up to five times larger than the actual physical size of the beam and it is significantly influenced by the presence of gas precursor. It is also demonstrated that the apparent beam size can be used as a reference value for optimization of the beam step during raster scanning. © 2015 American Vacuum Society. [<http://dx.doi.org/10.1116/1.4926388>]

## I. INTRODUCTION

Since the introduction of the Ga liquid metal ion source in the early 1980s, focused ion beam (FIB) instruments have been gaining increasing popularity and been established as invaluable tools in various fields of application. Some of the most typical applications are lamella preparation for transmission electron microscopy (TEM), slicing for 3D material characterization, circuit editing or chip failure analysis, and scanning ion microscopy. However, in recent years, FIB has come to be regarded as a manufacturing tool, which makes the question of instrument machining resolution a problem of increased research interest.<sup>1</sup> The machining resolution is highly dependent on the size and shape of the ion probe, which are defined by the current density distribution within the beam. The beam properties and its interaction with the sample have been demonstrated to be critical in advanced nanopatterning applications with very low dimensions.<sup>2,3</sup> At low currents, beam diameter of modern FIB systems can be as small as a few nanometers and is best described by a Gaussian function in the central parts and exponential functions in the edges, which widen faster.<sup>4</sup> These edges, often called tails, are normally of an intensity a few orders lower than the central part of the beam and for many applications in less sensitive materials they can be ignored.<sup>5</sup> There are several different indirect experimental methods of determining the current density distribution of FIB. Some of them are based on TEM analysis of FIB caused radiation damage,<sup>6,7</sup> and others use atomic force microscopy (AFM) for topography measurements<sup>8</sup> or scanning electron microscopy (SEM) observation of spot patterns exposed on polymer resist.<sup>9,10</sup> Despite the reduced accuracy, because of its simplicity, the most popular technique is the so called knife edge technique, which is based on a SEM characterization method

established by the American Society for Testing and Materials Standard.<sup>11</sup> In this method, the beam is swept across a sharp discontinuity (often a Faraday cup) and the change of ion current as a function of the beam position is used to estimate its size.<sup>12,13</sup> It can be shown that if the beam is assumed to have a Gaussian shape the full width at half maximum (FWHM) will correspond to the distance between 14% and 86% of the measured ion current change. A variation of the knife edge method is to sweep the beam across the interface of a heterostructure like AlGaAs/GaAs instead of a sharp discontinuity.<sup>14</sup>

All of the above methods provide a good estimation of the physical size of the beam and give indication of the quality of a specific instrument. However, the question of the instrument resolution remains open. FIB has a destructive nature to any specimen, and therefore, the full analysis of its imaging resolution involves elements of the information theory,<sup>15</sup> which is not investigated in the current paper. Although the machining (sputtering) resolution is often considered to be the physical beam size, this is highly influenced by the interaction of the ions with the specimen<sup>16</sup> and any species present in the vacuum chamber.<sup>17</sup> In practical terms this means that the sputtering resolution is dependent on the material of the specimen and the presence of any gas precursors. In this paper, this is addressed and investigated by defining the new term *apparent beam size* and developing a method of its evaluation by SEM measurements of FIB produced nanodots. Furthermore, this paper shows the importance of the apparent beam size when selecting the overlap in instruments with digital raster scan generators.

## II. APPARENT BEAM SIZE CONCEPT

### A. Overall concept definition

When ions from the beam penetrate a specimen material, they undergo multiple collisions with the bulk atoms. As a

<sup>a)</sup>Electronic mail: nikola.vladov@nottingham.ac.uk

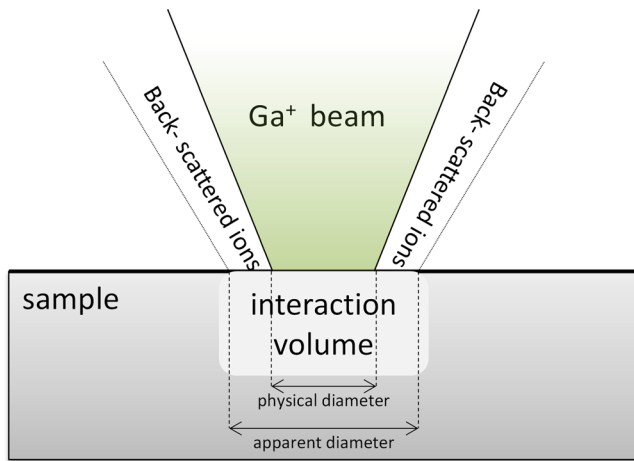


FIG. 1. (Color online) Apparent beam size concept. After multiple collisions with the target atoms many of the  $\text{Ga}^+$  ions are backscattered into the vacuum chamber, which effectively widens the beam.

result of the collisions, many of the bulk atoms are set into motion. They are called recoil atoms and they form a collision cascade. A large portion of the beam ions and recoiled atoms backscatter through the sample surface into the vacuum chamber.<sup>18</sup> Hence, the effective footprint of the beam, which causes damage to the surface is larger than the physical size of the beam, and here it is called *apparent beam size* (Fig. 1). The exact size and shape of the interaction volume of the ions with the solid is defined by the ion range, which is material dependent. In fact, the stopping of an ion is a stochastic process, and hence, a statistically broad distribution is observed for the values of the ion range of individual ions. Same as the beam current density, this distribution follows a Gaussian function, and therefore, it can be assumed that the beam footprint (apparent beam size) will have the same characteristic bell-like shape.

Another factor that can influence the nominal size and effectively the footprint of the beam is the presence of any gas in the vacuum chamber. The electrostatic forces between the gas molecules and the ions give rise to energy dependent scattering effects, which widen the beam. If the gas is a

chemical precursor for ion induced etching, an additional widening of the beam footprint will be initiated by the chemical reaction. The reaction can be initiated not only by the primary beam but also by the backscattered ions. All these processes are dependent on the current density distribution, and therefore, it is again assumed that the beam footprint (apparent beam size) takes the characteristic Gaussian bell-like shape.

In this paper, any possible beam tails and any artifacts that they might produce on the specimen surface are believed to be insignificant and are not taken into account. The beam is considered to leave a perfect Gaussian bell-like shape footprint and the apparent beam size is measured as the FWHM of the height of this footprint.

## B. Apparent beam size: Significance and applicability

The apparent beam size can be regarded as the smallest possible dot that FIB can produce at even infinitely short dwell time. It is the ultimate machining resolution. However, the apparent beam size also has another important role that becomes clear when analyzing the dose distribution during exposure. Because of the beam Gaussian shape when steering it in digital raster mode, the resulting dose is not always uniformly distributed. The distribution depends on the step, which is the smallest beam displacement and defines the size of exposed pattern pixels. The axisymmetric shape of the beam allows the formulation of the real three-dimensional problem in terms of much simpler two-dimensional equations. The Gaussian function of a real variable  $x$  is described by the following equation:

$$f(x) = \frac{1}{\sigma\sqrt{2\pi}} \exp - \left( \frac{(x-b)^2}{2\sigma^2} \right), \quad (1)$$

where  $\sigma$  is the standard deviation of the Gaussian distribution and  $b$  is the position of the center of the peak. To calculate the dose for an arbitrary chosen point A the superimposition of the Gaussians from all beam positions within the exposed pattern have to be summed. After multiplying by the probe current  $I$ , the current density  $J_A$  at the chosen point can be expressed as (Fig. 2)

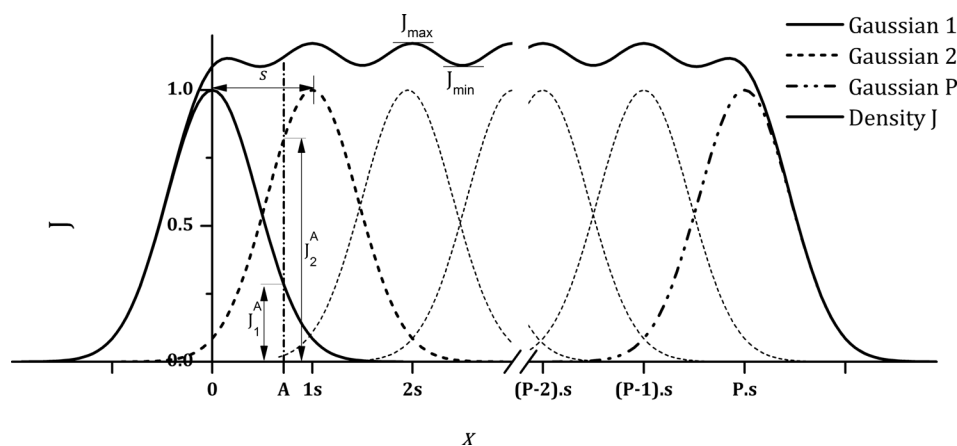


FIG. 2. Beam superimposition and spatial distribution of the current density  $J$ . In order to calculate the accumulated current density for a certain point the contribution from all beam positions has to be taken into account. The area below the solid line equals the sum of the areas closed by the individual Gaussians.

$$J_A = \sum_{i=1}^P \frac{I}{\sigma\sqrt{2\pi}} \exp - \left( \frac{(x_A - (i-1)s)^2}{2\sigma^2} \right), \quad (2)$$

where  $x_A$  is the position of point  $A$ ,  $P$  is the number of pixels in the exposed pattern, and  $s$  is the step. The resulting current density curve has a periodic character, which makes the ratio between its maximum and minimum value  $J_{\min}/J_{\max}$  a convenient criterion of the uniformity of the dose distribution. For a perfectly uniform distribution the density curve is a straight line and  $J_{\min}/J_{\max}$  equals 1. When calculating  $J_{\min}/J_{\max}$ , the current  $I$  cancels out so the ratio is actually only a function of the step  $s$  and the standard deviation  $\sigma$ . The graph from Fig. 3 shows that the dose distribution can be considered as perfectly uniform with 99.9% confidence for steps from zero up to  $1.54\sigma$ . The standard deviation can be directly related to the FWHM, and hence, it can be derived that to achieve uniform dose distribution the following condition needs to be met:

$$s \leq 0.65 \times \text{FWHM}. \quad (3)$$

If in the above equation the nominal beam size is used instead, the step size will be calculated to be much shorter than actually required.

### III. EXPERIMENTAL METHOD FOR APPARENT BEAM SIZE MEASUREMENT

#### A. Experimental setup

All experiments in this paper were performed on a Zeiss NVision 40 SEM/FIB Crossbeam workstation, which is equipped with a 30 kV Ga liquid ion source and Schottky field emitter electron source. The nominal pressure in the chamber is typically maintained at  $1 \times 10^{-6}$  mbar and falls to  $5 \times 10^{-5}$  when gas precursor is injected. Measurements of the apparent beam size for probe currents 40, 80, and 150 pA interacting with silicon (P type <111>), glassy carbon (GC) (Sigradur® K) and GC with inserted gaseous water were

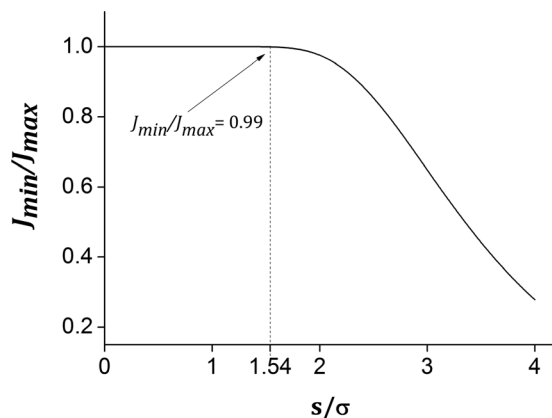


Fig. 3. Ratio of the minimum to the maximum value of the current density as a function of the step in terms of sigma. The dose distribution can be considered as uniform for steps up to  $1.54\sigma$ .

performed. The choice of these two materials was dictated by their excellent FIB machinability and difference in internal structure. Water was chosen because of its capability to act as a chemical precursor for etching of carbon based materials.

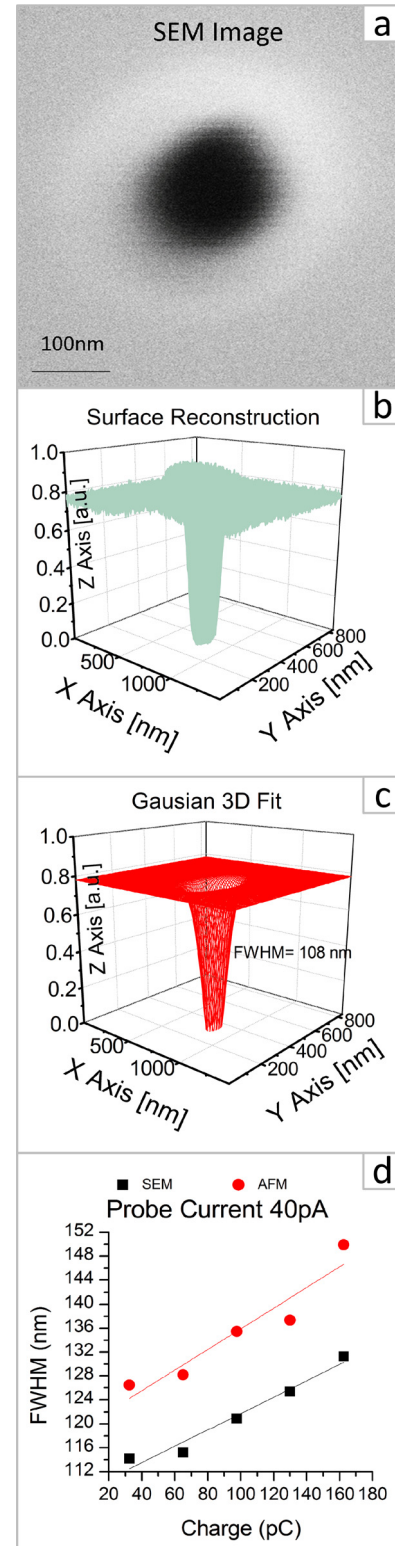


Fig. 4. (Color online) Apparent beam size measurement method. The gray levels from an SEM image (a) are translated into height to reconstruct the surface (b) of FIB produced nanodots. The surface is fit to a Gaussian function (c), which FWHM is extrapolated for zero charge (d). The AFM curve is for validation only.

## B. Measurement method

The method for apparent beam size measurement is outlined in Fig. 4. First, a series of nanodots are FIB sputtered on the surface of a well-polished specimen by applying a range of exposure doses. The dose needs to be large enough so that the dots can be visualized using a SEM. Then, based on the pixel gray scale from the SEM image, a 3D plot representing the FIB footprint is reconstructed. The lateral scale of the plot is calculated from the magnification of the SEM and the height is converted into arbitrary units. Consequently, the resulting surface is fitted to a 2D Gaussian function and its FWHM is calculated. A XY chart of the FWHM as a function of the applied dose is drawn. The chart is extrapolated to zero dose, and the resulting FWHM is taken as the apparent beam size. The procedure is applied to different probe currents, specimen materials, and gas precursors that are of interest. The exposure and the measurement of every dot are repeated five times in order to avoid errors caused by possible instabilities or misalignment of the electro-optics system.

It is important to keep the exposure dose low enough to avoid any possible redeposition effects. Since the beam is not scanned but kept at a point and the dots spread across an unspecified area, the traditional definition of dose is inapplicable. What can be used instead is the total electric charge delivered to the specimen, which is measured in pA and can be calculated by simply multiplying the exposure time by the probe current.

Because of the angle dependence of secondary electrons, the edges of the nanodots always appear brighter in the SEM images. To avoid errors in the fitting of the Gaussian function when translating the gray levels into height, a threshold corresponding to the specimen surface plane has to be set.

In order to check the reliability of the above procedure some arbitrarily chosen measurements were repeated by AFM imaging. The difference between the SEM and the AFM results ranges between 1% and 13% with the AFM FWHM being always larger than the SEM. This could possibly be explained by existing limitations in the AFM measurement of sidewall angles and the difficulties of the SEM to register signal from the central, deepest, part of the FIB

footprint. A single beam uncoated silicon cantilever ending on a standard shaped tip with a radius of 7 nm was used for the AFM imaging. The front side of the tip has an angle of 25° and the back side angle is 15°.

It was found that the minimum charge, which still produces nanodots big enough to be SEM visualized, is 32.5 pC. To obtain enough data points for the FWHM extrapolation, the charge was incrementally increased to 162.5 pC in steps of 32.5 pC. High resolution 1024 × 724 SEM images of each nanodot were produced with such a magnification that every pixel corresponds to 1.4 nm length. After reconstruction of the surface, a *chi-square minimization* method was used to build the 2D Gaussian function. The fitting tolerance was set to 1 nm that typically allowed convergence in about 40 iterations with  $R^2$  value above 0.9 and an error of less than 5% for the calculated parameters.

## IV. EXPERIMENTAL RESULTS AND DISCUSSION

### A. Beam measurement

Figure 5 presents the apparent beam size measured for several combinations of probe current, specimen material, and gas precursor. A linear extrapolation was applied to the points which represent the averaged value of the FWHM in the XY plane. Every dot exposure and measurement were repeated five times in order to avoid errors from misalignment of the electro-optics system. However, the difference between measurements was found to be less than 1%.

Clearly, the size of the dots cannot grow infinitely with the increase of the charge and therefore some different extrapolation (e.g., exponential) would provide more accurate results. However, to do this, a broader range of data with dwell times exceeding any practical applications are required. Additionally, the long dwell times would cause redeposition effects and aspect ratios of the dots impossible to measure by SEM or AFM.

Table I provides a summary of the extrapolated values of the apparent beam size and compares them to the nominal values of the beam measured by the instrument manufacturer using the knife edge method. For most cases, the difference would be larger than five times even if the fitting and extrapolation error was subtracted from the apparent beam size. As

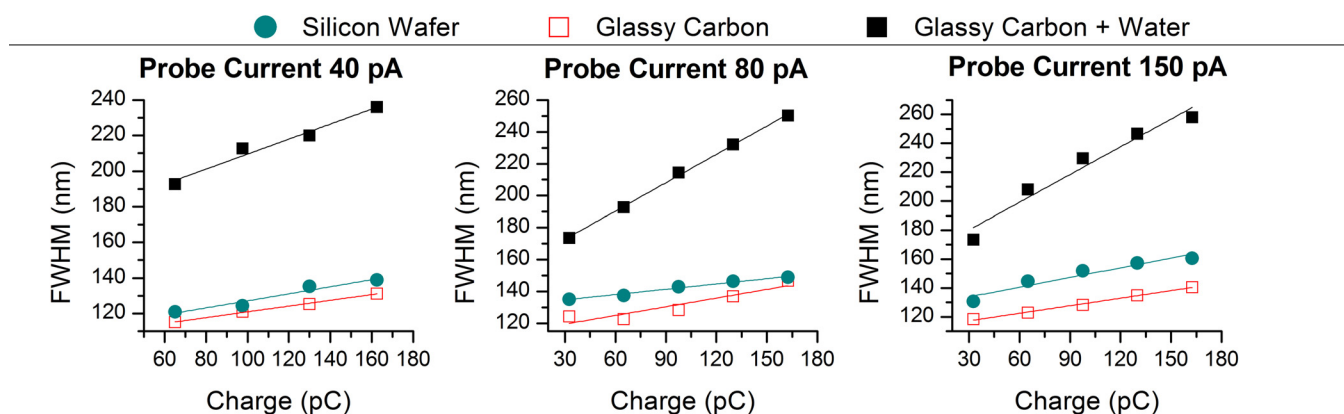


Fig. 5. (Color online) Apparent beam diameter for a range of probe currents and electric charges in silicon, glassy carbon, and glassy carbon with water gas precursor. The straight lines are linear fit of the experimental points obtained from analysis of 2D SEM images.

TABLE I. Apparent beam size for infinitely small dose compared to the beam size measured by the knife edge method. The error is from the fitting and the extrapolation procedures.

Probe current (pA)	Apparent beam diameter (nm)						Knife edge diameter (nm)
	Glassy carbon		Silicon wafer		Glassy carbon +H <sub>2</sub> O		
	FWHM	Error	FWHM	Error	FWHM	Error	
40	108.0	1.6	111.6	2.9	153.1	7.5	19
80	114.0	4.3	131.4	1.0	154.9	1.2	22
150	117.1	0.7	127.1	3.9	161.0	8.4	29

anticipated, the apparent beam is wider in the presence of gas precursor molecules, which act as scattering centers. The values for GC and silicon are similar, and this is coherent with their close stopping power and ion range, which can be calculated by using any software tool like the stopping and range of ions in matter (SRIM).<sup>19</sup> It draws attention that in the case of added gas precursor, the gradient of the lines from Fig. 5 is larger. Although this requires further investigation, it could be speculated that the cause is the concentration of precursor molecules, which increases with the time. Lower probe currents require longer exposure time.

## B. Factors influencing the apparent beam size

Aside from the probe current, one of the most significant factors that can influence the apparent beam size is the energy of the beam. The energy affects the electrostatic lenses and their focusing strength. However, there are some more fundamental effects to be considered, which are related to the interaction of the ions with the target material. The depth, size, and shape of the interaction volume depend on the ion energy. SRIM simulations can be used to visualize the collision cascade. At 30 kV, even for an idealized Ga point source, the collision cascade spreads over an area of tens of nanometers. This can be linked to the minimum possible apparent beam size, which by definition is directly related to the interaction volume. For low probe currents and energies, the difference between the physical size of the beam and the apparent beam size is greatest (see Fig. 6). For

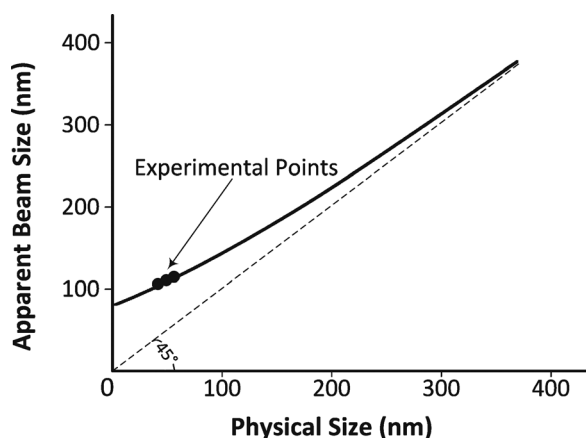


Fig. 6. Anticipated trend of the apparent beam size compared to the physical (knife edge) beam size. The experimental data are for glassy carbon in Table I.

larger currents, the physical size of the beam is comparable in size with the collision cascade and therefore the apparent beam size. The general trend of this relationship is suggested in Fig. 6, which includes some of the experimental points from this paper. The figure also provides a good comparison between the apparent beam size and the commonly measured knife edge diameter since it is a close approximation of the physical beam size. It is somewhat harder to envisage the behavior of the apparent beam size as a function of the energy alone. Higher energy leads to a larger interaction volume, but this is offset by a deeper collision cascade, which might result in less damage to the surface. As already discussed, the energy influences the lenses' focusing strength too.

## C. Apparent beam size and dose distribution effects

To validate the relation between the apparent beam size and the dose uniformity, which is defined by Eq. (3), a series of boxes with growing step were FIB sputtered in a silicon specimen. For all of them, 150 pA probe current was used with dwell time of 1.6  $\mu$ s and dose of 0.2  $\mu$ As/ $\mu$ m<sup>2</sup>. To keep the dose constant when changing the step, the number of loops was adjusted as recorded in Table II. The table also includes the anticipated dose uniformity based on the measured apparent beam size. The dose uniformity is calculated as the ratio of the minimum to the maximum value of the current density  $J_{\min}/J_{\max}$  using Eq. (2). An SEM image of the boxes is shown in Fig. 7. The length of the step for box number 3 can be considered as a critical value as this is the box where the stripes on the bottom surface caused by an uneven dose distribution just become visible. This is in good agreement with Eq. (3), which shows that for a 150 pA probe current applied on silicon, the step must be smaller than 83 nm. The condition is satisfied only for the smooth boxes 1 and 2, which were exposed with step providing uniformity

TABLE II. Exposure parameters and predicted uniformity for the boxes from Fig. 7. The probe current and the exposure are kept constant at 150 pA and 0.2  $\mu$ As/ $\mu$ m<sup>2</sup>, respectively.

	Box 1	Box 2	Box 3	Box 4	Box 5	Box 6
Step (nm)	65	80	95	110	125	140
Loops	3521	5333	7521	10083	13021	16333
Uniformity (%)	100	99.99	99.32	96.57	90.28	80.92

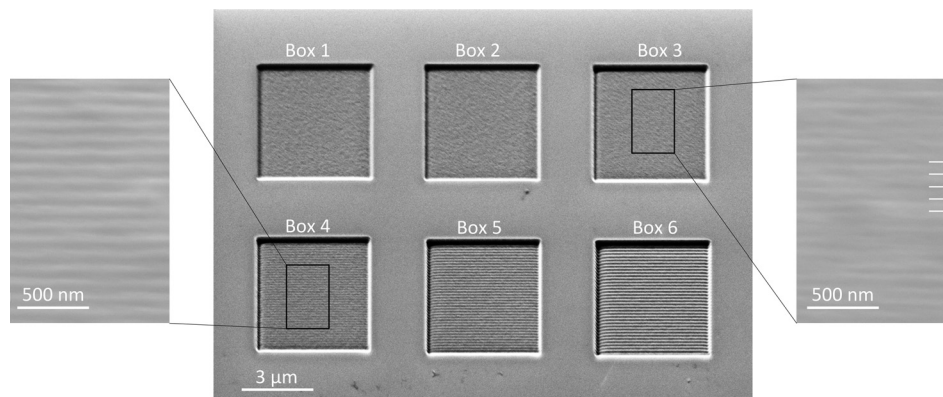


FIG. 7. FIB sputtered boxes in silicon showing the effects of uneven dose distribution. While the beam step is incrementally increasing by 15 nm for each box, the current and the does are kept constant. Exact parameters as indicated in Table II.

better than 99.9%. This experiment demonstrates that the apparent beam size can be successfully used to predict accurately whether or not the FIB sputtering will result in a smooth final surface. However, it cannot be assumed that the final surface will match the wavelike shape from Fig. 2 as during long exposures redeposition effects and varying removal rate caused by the local geometry will arise.

## V. CONCLUSIONS

Although the physical beam size of FIB instruments is often considered to be their machining resolution, the smallest producible nanodots can be up to five times larger. The size of these dots has been linked to the value of the *apparent beam size* as introduced and defined in this paper. By reconstructing 3D profiles from planar SEM images, it has been demonstrated that the apparent beam size is material dependent and is influenced by the presence of gas precursor in the vacuum chamber. Furthermore, the apparent beam size has proven to be very valuable in the choice of scanning parameters providing uniform dose distribution with sputtering resulting in smooth final surface. To achieve a smooth surface, the scanning step has to be 0.65 parts of the apparent beam size or smaller.

In this work, the beam current distribution has been assumed to take an ideal axisymmetric Gaussian shape. However, further improvement of the analysis might be achieved if the fitting function is split to Gaussian and exponential parts, which can better represent beam tails. In combined SEM/FIB systems, the 3D profile reconstruction can be done in real time, enabling automatic iterative alignment of the ion optical system aberrations.

## ACKNOWLEDGMENT

The authors wish to acknowledge the Engineering and Physical Sciences Research Council (EPSRC) for their financial support of the research.

- <sup>1</sup>R. M. Langford, P. M. Nellen, J. Gierak, and Y. Fu, *MRS Bull.* **32**, 417 (2007).
- <sup>2</sup>M. Rommel, A. J. Bauer, and L. Frey, *Microelectron. Eng.* **98**, 242 (2012).
- <sup>3</sup>A. Joshi-Imre and S. Bauerdick, *J. Nanotechnol.* **2014**, 170415.
- <sup>4</sup>M. Sato and J. Orloff, *J. Vac. Sci. Technol. B* **9**, 2602 (1991).
- <sup>5</sup>I. M. Templeton and H. G. Champion, *J. Vac. Sci. Technol. B* **13**, 2603 (1995).
- <sup>6</sup>S. Tan, R. Livengood, Y. Greenzweig, Y. Drezner, and D. Shima, *J. Vac. Sci. Technol. B* **30**, 06F606 (2012).
- <sup>7</sup>G. B. Assayag, C. Vieu, J. Gierak, P. Sudraud, and A. Corbin, *J. Vac. Sci. Technol. B* **11**, 2420 (1993).
- <sup>8</sup>A. Lugstein, B. Basnar, G. Hobler, and E. Bertagnolli, *J. Appl. Phys.* **92**, 4037 (2002).
- <sup>9</sup>S. Shukuri, Y. Wade, M. Tamura, K. Umamura, and T. Ishitani, *J. Electrochem. Soc.* **134**, 1536 (1987).
- <sup>10</sup>R. L. Kubena and J. W. Ward, *Appl. Phys. Lett.* **51**, 1960 (1987).
- <sup>11</sup>ASTM International, [www.astm.org/database.cart/historical/e986-97.htm](http://www.astm.org/database.cart/historical/e986-97.htm).
- <sup>12</sup>T. Ishitani, H. Tamura, and H. Todokoro, *J. Vac. Sci. Technol.* **20**, 80 (1982).
- <sup>13</sup>S. A. Rishton, S. P. Beaumont, and C. D. W. Wilkinson, *J. Phys. E: Sci. Instrum.* **17**, 296 (1984).
- <sup>14</sup>H. Arimoto, A. Takamori, E. Miyauchi, and H. Hashimoto, *Jpn. J. Appl. Phys., Part 2* **22**, L780 (1983).
- <sup>15</sup>J. Orloff, L. W. Swanson, and M. Utlaut, *J. Vac. Sci. Technol. B* **14**, 3759 (1996).
- <sup>16</sup>P. W. H. de Jager and P. Kruit, *J. Vac. Sci. Technol. B* **14**, 3753 (1996).
- <sup>17</sup>M. Komuro, *Appl. Phys. Lett.* **52**, 75 (1988).
- <sup>18</sup>M. Nastasi, J. Mayer, and J. Hirvonen, *Ion-solid Interactions: Fundamentals and Applications* (Cambridge University, Cambridge, 1996).
- <sup>19</sup>J. F. Ziegler "SRIM," Last accessed 12 February 2015, [www.srim.org](http://www.srim.org).